

A near-UV reconnaissance of metal-poor massive stars

Chris Evans · Wagner Marcolino ·
Jean-Claude Bouret · Miriam Garcia

Accepted: 8 August 2023

Abstract We use synthetic model spectra to investigate the potential of near-ultraviolet (3000-4050 Å) observations of massive O-type stars. We highlight the He I λ 3188 and He II λ 3203 pair as a potential temperature diagnostic in this range, supported by estimates of gravity using the high Balmer series lines. The near-ultraviolet also contains important metallic lines for determinations of chemical abundances (oxygen in particular) and estimates of projected rotational velocities for O-type spectra. Using the model spectra we present performance estimates for observations of extragalactic massive stars with the Cassegrain U-Band Efficient Spectrograph (CUBES) now in construction for the Very Large Telescope. The high efficiency of CUBES will open-up exciting new possibilities in the study of massive stars in external galaxies. For instance, CUBES will provide new insights into the physical properties of O-type stars, including oxygen abundances, in metal-poor irregular galaxies at ~ 1 Mpc from integrations of just 2-3 hrs. Moreover, CUBES will bring quantitative spectroscopy of more distant targets within reach for the first time, such as the O-type star ($V \sim 21.5$ mag) in Leo P (at 1.6 Mpc) in only half a night of observations.

C. Evans
European Space Agency (ESA), ESA Office, Space Telescope Science Institute, 3700 San Martin Drive, Baltimore, MD 21218, USA
E-mail: chevans@stsci.edu

W. Marcolino
Universidade Federal do Rio de Janeiro, Observatório do Valongo, Ladeira Pedro Antônio, 43, CEP 20.080-090, Rio de Janeiro, Brazil

J.-C. Bouret
Aix-Marseille Univ, CNRS, CNES, LAM, Marseille, France

M. Garcia
Centro de Astrobiología, CSIC-INTA, Crtra. de Torrejón a Ajalvir km 4, E-28850, Torrejón de Ardoz (Madrid), Spain

Keywords instrumentation: spectrographs · stars: early-type · galaxies: Local Group · galaxies: individual: Leo P

1 Introduction

Ground-based spectroscopy of OB-type stars has traditionally been obtained in the $\lambda 3950\text{--}4750\text{\AA}$ range for spectral classification (e.g. [1]) and estimates of physical parameters (temperatures, gravities), and of the $\text{H}\alpha$ line to investigate their stellar winds (e.g. [2]). In contrast, the shorter wavelengths accessible from the ground, down to the atmospheric cut-off, have received significantly less attention, partly due to the challenges of the reduced atmospheric transmission combined with the limited efficiency of available instrumentation.

Development of the Cassegrain U-Band Efficient Spectrograph (CUBES) instrument for the Very Large Telescope (VLT) provided us with the motivation to investigate the potential of observations of massive stars in the near ultraviolet (UV). The CUBES design offers a potential tenfold gain in end-to-end efficiency at $\lambda < 3400\text{\AA}$ (incl. the telescope and atmosphere) compared to the existing Ultraviolet and Visible Echelle Spectrograph (UVES). In brief, the CUBES design provides a spectral resolving power of $R \geq 20,000$ over the $3000\text{--}4050\text{\AA}$ range, with provision of a second, lower-resolution option with $R \sim 7,000$ [3].

Here we investigate the potential performance of CUBES for studies of massive stars. In Sect. 2 we briefly review past studies of massive stars shortwards of 4000\AA . Motivated by the presence of a relatively strong He II line ($\lambda 3203$) and a range of He I lines, in Sect. 3 we use synthetic model spectra to qualitatively investigate the sensitivity of near-UV lines to the physical parameters of massive stars. In Sect. 4 we focus on the possibility of estimating oxygen abundances in massive stars from near-UV observations. In Sect. 5 we investigate the potential performance of CUBES to study massive stars in Local Group galaxies and beyond, with concluding remarks given in Sect. 6.

2 Near-ultraviolet spectroscopy of massive stars

An early ground-based study of massive stars at $\lambda < 4000\text{\AA}$ used photographic observations of ϵ Ori (B0 Ia), which included a detailed linelist that extended as far bluewards as 3550\AA [4]. A first quantitative investigation of the He I $\lambda 3188$ and He II $\lambda 3203$ lines employed photographic observations from the 2.2-m telescope on Mauna Kea of 19 O- and B0.5-type stars [5]. This included equivalent width-measurements of both lines in the sample of stars, and comparisons with the predictions of non-LTE model atmospheres for He I $\lambda 3889$ and He II $\lambda 3203$, finding generally good agreement for the trend of the He I lines and the values for the He II line (except for the two hottest stars). Given the strong response to temperature of both lines, this was a first indication of the potential of these two lines to be used in tandem as a temperature diagnostic. The only other example known to us of observations in this region

prior to the use of digital detectors is observations of the He I $\lambda 3188$ line in ~ 30 early-type stars with the *Copernicus* satellite [6].

Digital detectors transformed observational astronomy, but their performance in the near UV has still been a limiting factor compared to longer wavelengths, and so there remain relatively few studies of massive stars in this region. Observations covering 3250–4750 Å of massive O-type and Wolf–Rayet stars in NGC 3603 with the Faint Object Spectrograph on the *Hubble Space Telescope* (*HST*) revealed some of the key features in the near UV [7]. Shortwards of 4000 Å, the O-type spectra are dominated by the high Balmer series until the Balmer limit, with a He I line at $\lambda 3820$. Going to even shorter wavelengths, in the hottest (O3-type) stars in the *HST* observations, absorption from O IV $\lambda\lambda 3381$ –85, 3412 and N IV $\lambda\lambda 3479$ –83–85 are also seen, with the N IV blend displaying a strong P Cygni profile in the hydrogen-rich WN-type spectra. Examples of some of the weak He I lines present in the 3800–4000 Å range can also be seen in slightly higher-resolution (~ 2 Å) spectroscopy of four late O-type supergiants (from [8]).

To illustrate some of the spectral lines present in this range, in Fig. 1 we show the far-blue UVES spectrum of HDE 269896 (taken from [9]), smoothed and rebinned to the high-resolution mode of CUBES ($\Delta\lambda = 0.14$ Å, sampled by 2.3 pixels, so 0.06 Å/pixel).

The region below ~ 3400 Å in the UVES data was of limited use because of low signal-to-noise (S/N) in the shortest-wavelength echelle orders, but at longer wavelengths the data give a good example of some of the features present in massive stars in the CUBES range. In practice, degrading the spectrum to the $R \sim 7,000$ of the low-resolution mode has little qualitative impact on the final spectrum shown in Fig. 1 given the (astronomical) broadening of the lines.

Classified as ON9.7 Ia+ (and with $\log(L/L_{\odot}) \approx 6$) the UVES data of HDE 269896 reveal the high Balmer series and a plethora of He I lines, together with weak emission lines from Si III ($\lambda 3487$, 3590, 3807), Si IV ($\lambda 3762$ and 3773) and Al III ($\lambda 3602$) produced in its strong stellar wind (see [9]). The presence of lines from two ionisation stages of silicon offers a potential temperature diagnostic in the CUBES region, albeit very dependent on the adopted stellar parameters (including the wind) when the lines are in emission.

To illustrate the ability of sophisticated model atmospheres and spectral synthesis to reproduce this region in O-type spectra (including the higher-order members of the Balmer series), in red in Fig. 1 we overplot the adopted CMFGEN model (see [10]) for this star from [9]. The adopted parameters were an effective temperature, $T_{\text{eff}} = 27,500$ K, $\log g = 2.7$, and a rotational velocity of $v \sin i = 70 \text{ km s}^{-1}$ (see [9] for further details of the model parameters, which necessitated a detailed treatment of the wind in this luminous supergiant star).

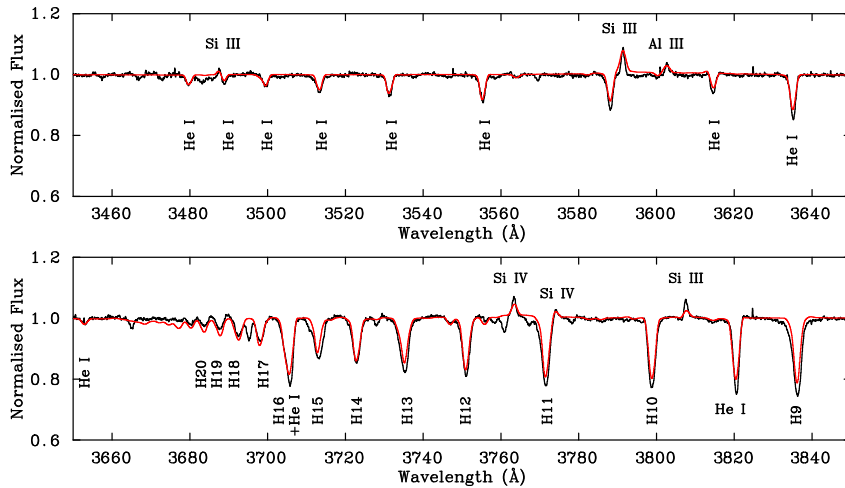


Fig. 1 *Black spectrum*: UVES spectrum of HDE 269896, an ON9.7 Ia+ star in the Large Magellanic Cloud. The data have been smoothed and rebinned to match the CUBES high-resolution mode (with $R \sim 22,000$). Identified lines in the upper panel are: Al III λ 3602; He I λ 3479, 3488, 3499, 3513, 3531, 3554, 3614, 3634; Si III λ 3487, 3590. In addition to the high Balmer lines (H9–20), identified lines in the lower panel are: He I λ 3652, 3820; Si III λ 3807; Si IV λ 3762, 3773. *Red spectrum*: Adopted CMFGEN model from a combined UV and optical analysis of the UVES data (taken from [9], see text for details).

3 Diagnostic lines in the near UV

To investigate the sensitivity of different spectral lines in the near UV to physical parameters such as temperature and gravity, we used synthetic spectra from the extensive OSTAR2002 grid¹ of line-blanketed, non-LTE, plane-parallel, hydrostatic model atmospheres calculated with the TLUSTY code [11].

3.1 LMC metallicity: Temperature trends

The metallicity of the Large Magellanic Cloud (LMC) is approximately half solar and we have a good understanding of stellar properties from analysis of data at other wavelengths (e.g. [12]). We therefore first considered the $0.5 Z_{\odot}$ models from the OSTAR2002 grid as example sub-solar models with which to investigate the CUBES domain.

We initially considered models with $\log g = 4.0$, that are typical of the gravities estimated for dwarfs [14]. The TLUSTY grid has models from $T_{\text{eff}} = 27,500$ to 55,000 K (in steps of 2,500 K). Using the effective temperature – spectral type relations derived from analysis of O- and B-type dwarfs in the LMC [14, 15], we can map the TLUSTY models to approximate spectral types.

¹ <http://tlusty.oca.eu/Tlusty2002/tlusty-frames-OS02.html> in which abundances in the OSTAR2002 grid are scaled relative to solar values from [13].

The near-UV and visible ranges are shown for eight model spectra in Figs. 2 and 3, respectively. Each model spectrum in the figures has been convolved with a rotational-broadening function of $v \sin i = 100 \text{ km s}^{-1}$ to mimic real targets compared to the unbroadened models. Note that $v \sin i$ of order 100 km s^{-1} then dominates the broadening of the line profiles, such that convolving the models to either the high- or low-resolution modes of CUBES has a limited impact compared to the spectra shown in the figure.

Our motivations to show the visible region of the models is twofold. Firstly, to investigate if there are near-UV lines in the same models that can then be used to delineate similar trends as in the temperature (spectral type) sequence in Fig. 3. Secondly, the models shown illustrate some of the key classification criteria in O- and early B-type stars (see [1, 16]). For instance, the weakening of the He I lines when moving to hotter temperatures (earlier spectral types), such that the He I $\lambda 4471$ line is very weak by O3 ($T_{\text{eff}} \approx 45,000 \text{ K}$), and the weakening of the He II lines as we move to cooler temperatures (later spectral types), such that the Si III triplet is stronger than He II $\lambda 4542$ by B0. The $T_{\text{eff}} = 40,000 \text{ K}$ model is also a useful classification anchor point in terms of the He I/He II ratios for the $\lambda 4026/\lambda 4200$ and $\lambda 4388/\lambda 4542$ pairs, corresponding to a classification of $\sim \text{O6}$.

To complement the UVES data of HDE 269896, in Fig. 2 we show the near-UV ($\lambda < 3450 \text{ \AA}$) spectra for the same models as shown in Fig. 3. The primary features of interest, in terms of their potential usefulness for spectral classification and determination of physical parameters are the He I $\lambda 3188$ and He II $\lambda 3203$ lines (previously studied by [5]). The He I line is absent for the hottest spectra and increases in strength down the temperature sequence, while the He II changes in the opposite sense. The lines are closest to being equivalent in the $T_{\text{eff}} = 32,500$ model, which would be classified as approximately O9.7 V from comparison of its blue-visible spectrum (Fig. 3) to published spectral standards [16], although the point at which the line intensities are equal is slightly cooler.

This region is also rich with O III absorption lines, as well as pairs of lines from Si III and Si IV and several O IV lines in the hottest spectra. As at the longer wavelengths shown in Fig. 1, the presence of two ionisation stages in this region (from multiple species) offers alternative potential diagnostics of temperature.

In this first exploration, with relatively modest rotational broadening ($v \sin i = 100 \text{ km s}^{-1}$), we have followed the general classification approach for digital spectral of considering the central line depths rather than the line intensities (equivalent widths). Once empirical data is available for a broad range of massive stars in this spectral range, a more robust morphological treatment will be required in the future, which e.g. takes into account effects such as rotational broadening (e.g. [17], see also the discussion by [18]).

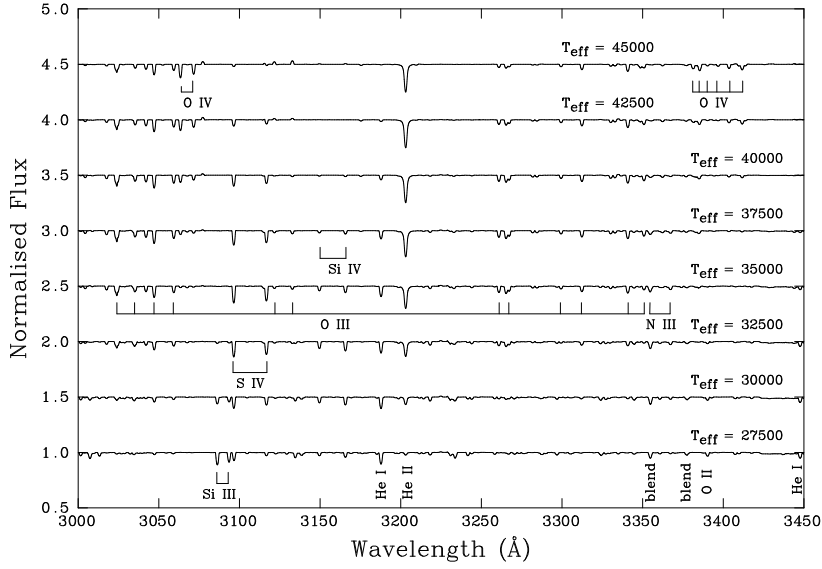


Fig. 2 Synthetic near-UV spectra from the TLUSTY $Z=0.5Z_{\odot}$ OSTAR2002 grid, which have been convolved with a rotational-broadening function of $v \sin i = 100 \text{ km s}^{-1}$. Identified lines are: He I $\lambda\lambda 3188, 3448$; He II $\lambda 3203$; N III $\lambda\lambda 3354, 3367$ (where the former is blended with Ne II 3355); O II $\lambda\lambda 3390$; O III $\lambda\lambda 3024, 3035, 3047, 3059, 3122, 3133, 3261, 3267, 3299, 3312, 3341, 3351$; O IV $\lambda\lambda 3063, 3072; 3381, 3385, 3390, 3397, 3404, 3410\text{-}12\text{-}14$; Si III $\lambda\lambda 3086, 3093$; Si IV $\lambda\lambda 3150, 3166$; S IV $\lambda\lambda 3097, 3118$. Two blends are also identified at $\lambda 3355$ (He I and Ne II) and $\lambda 3377$ (O II and Ne II).

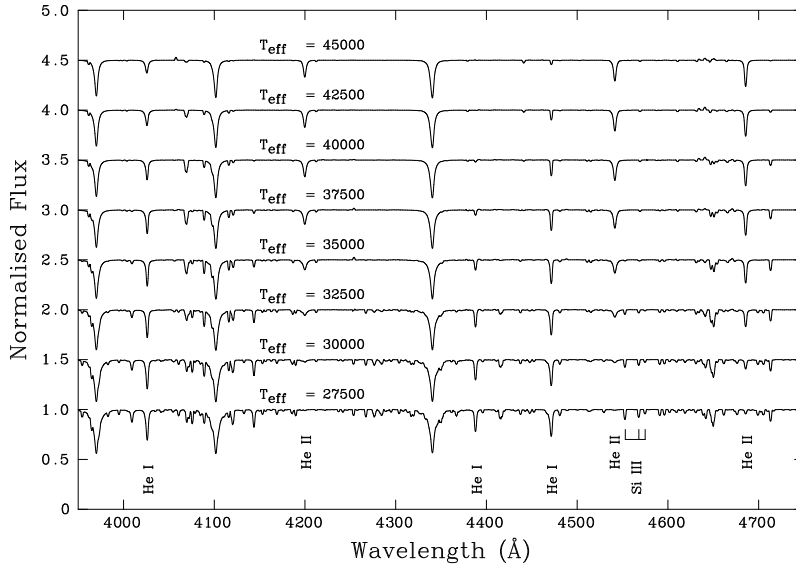


Fig. 3 Synthetic spectra from the TLUSTY $Z=0.5Z_{\odot}$ OSTAR2002 grid for the traditional classification domain. The spectra have been convolved with a rotational-broadening function of $v \sin i = 100 \text{ km s}^{-1}$. The identified lines are some of those used for classification of O-type spectra, namely: He I $\lambda\lambda 4026$ (blended with He II at the hottest temperatures), 4388, 4471; He II $\lambda\lambda 4200, 4542, 4686$; Si III $\lambda\lambda 4552\text{-}68\text{-}75$.

3.2 LMC metallicity: Stellar gravities

The $\lambda 3188/\lambda 3203$ line ratio looks potentially interesting in the context of (approximate) spectral classification and estimates of T_{eff} , but if we were limited to CUBES observations alone of a given target we must also consider how to constrain its gravity (as well as the possible impact that it has on the $\lambda 3188/\lambda 3203$ ratio). As demonstrated in Fig. 1, the CUBES range contains the high Balmer series lines (plus the H8 and H ϵ lines not shown in the figure). The profile wings of the Balmer series are generally excellent diagnostics of stellar gravity, and the high Balmer lines could be used to constrain the gravities of CUBES targets. With crossed-dispersed instruments such as UVES and X-Shooter, correction of the echelle blaze function and stitching together the different echelle orders can be challenging in the 3650-3900 Å region, where the wings of the Balmer lines can overlap and it is difficult to accurately define a continuum. An advantage of the CUBES design is the continuous spectrum from each of its two arms, provided by having only one dispersing element (in each arm) operating in first order [3], i.e. no echelle orders to combine in the data reduction.

To illustrate the diagnostic potential of the Balmer lines in this regard, in Fig. 4 we show models for $T_{\text{eff}} = 35,000$ K (typical of a late O-type star) for three gravities: $\log g = 3.5$ (a typical value for an O-type giant in the LMC, e.g. [19]), 4.0 and 4.5, spanning from shortwards of the Balmer limit up to the H8 line. We recognise the challenges of the blending of the higher-series lines (particularly for noisy data), but note that the H8 line is relatively isolated, and the CUBES range (which extends further redwards to 4050 Å) also includes the H ϵ line. While the latter is blended with the interstellar Ca II *K* line at $\lambda 3968$, its redward wing could be used to provide further constraints.

The adopted gravity does have an impact on the strengths of the He I $\lambda 3188$ and He II $\lambda 3203$ lines (as shown in Fig. 5), with the former being stronger and the latter being weaker at higher gravities. As such, good S/N across the full CUBES range will be critical to ensure the maximum information is available, but the key point is that there are potential diagnostics available of both temperature and gravity.

A caveat of our approach in using the TLUSTY models is that the effects of stellar winds are not included, which would be expected to modify the appearance of the emergent spectra. However, we note that the winds of O-type giants and dwarfs at sub-solar metallicity are generally weak, and the TLUSTY models are sufficient for our qualitative objectives here.

3.3 Low-metallicity models ($Z = 1/30 Z_{\odot}$)

The LMC-like models described above will be relevant for future CUBES targets in external galaxies, but the real push is to extend studies to lower metallicities than currently possible (see [20]). A significant effort over the past 20 years has gone into quantifying the impact that metallicity has on the evolu-

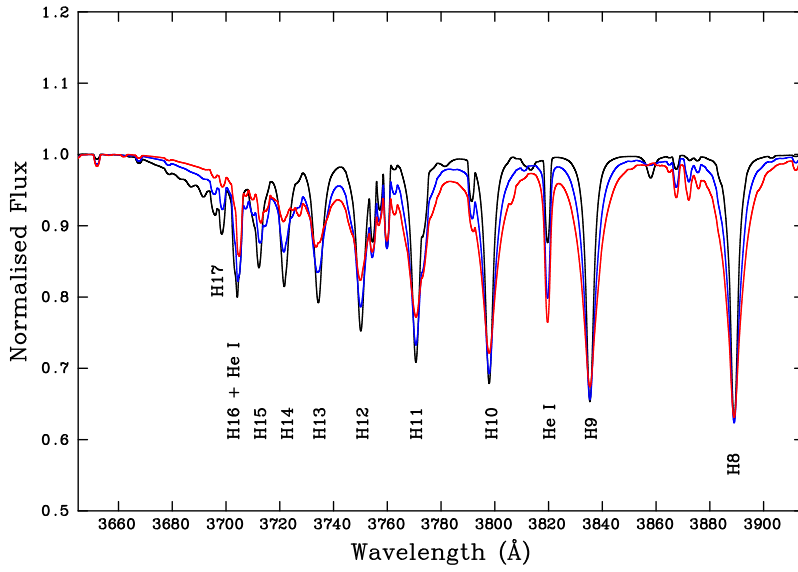


Fig. 4 Synthetic spectra from the TLUSTY $Z = 0.5Z_{\odot}$ OSTAR2002 grid for the high Balmer lines for $T_{\text{eff}} = 35,000$ and three gravities: $\log g = 3.5$ (black spectrum), 4.0 (blue) and 4.5 (red). Identified lines are the same as those in Fig. 1, plus the H8 line ($\lambda 3889$).

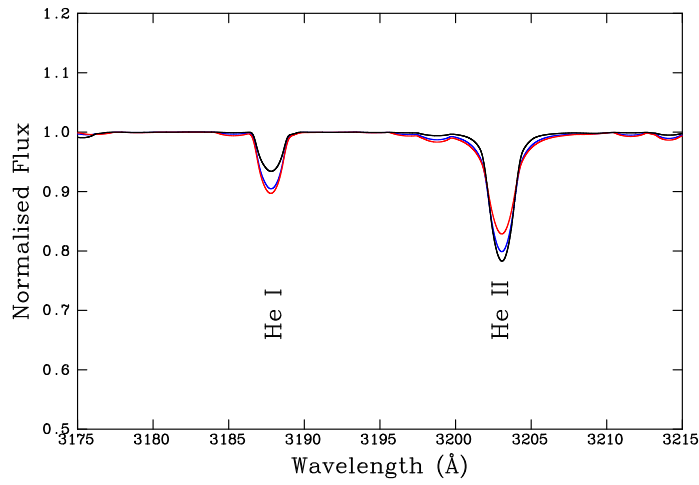


Fig. 5 Synthetic TLUSTY spectra ($Z = 0.5Z_{\odot}$) for the He I $\lambda 3188$ and He II $\lambda 3203$ lines for $T_{\text{eff}} = 35,000$ and three gravities: $\log g = 3.5$ (black spectrum), 4.0 (blue) and 4.5 (red).

tion of massive stars, so that we can improve stellar-evolution and population-synthesis models to more accurately reproduce the massive-star populations seen in both the local Universe and high-redshift, star-forming galaxies. Necessarily, most efforts have focused on massive stars in the Milky Way, LMC and the Small Magellanic Cloud (SMC), spanning a range of metallicities from that of the solar neighbourhood down to approximately one-fifth solar in the SMC. This puts limits on our ability to test model predictions at lower metallicities, and requires (uncertain) extrapolations.

High-efficiency, multi-object spectrographs, such as the FOcal Reducer/low dispersion Spectrograph 2 (FOR2) on the VLT, have provided first insights (at $R \sim 1,000$) into limited numbers of massive stars in more distant systems, with nebular oxygen abundances of $\sim 0.15Z_{\odot}$, namely: IC 1613 at 0.7 Mpc, WLM at 0.9 Mpc, and NGC 3109 at 1.2 Mpc. However, a key motivation to improve our understanding of the physical properties of massive stars, and their contribution to galaxies in the early Universe, is to directly observe stars at even lower metallicities. Example targets in this context include: Sextans A ($0.1Z_{\odot}$ at 1.3 Mpc), SagDIG ($0.05Z_{\odot}$ at 1.1 Mpc), Leo P ($0.03Z_{\odot}$ at 1.6 Mpc) and, ultimately, IZw18 ($0.02Z_{\odot}$ at 18.9 Mpc).

To investigate the spectral lines in such extremely metal-poor stars, we have used the $0.03Z_{\odot}$ models from the TLUSTY OSTAR2002 grid. As a first comparison with the LMC-like models, the near-UV and visible regions for the $0.03Z_{\odot}$ models are shown in Figs. 6 and 7, respectively. Echoing the shift to higher temperatures for a given zero-age main-sequence mass at lower metallicity (e.g. [21], and references therein), note the He I/He II line ratios in the $T_{\text{eff}} = 40,000$ K model compared to that in Fig. 3. The $T_{\text{eff}} = 40,000$ K model for $0.03Z_{\odot}$ would be classified as a slightly later type than that for the $0.5Z_{\odot}$ model. Similarly, the He I $\lambda 4471$ line is stronger in the $0.03Z_{\odot}$ model. In short, a spectrum classified as, e.g. O3 or O6, at very low metallicity (e.g. in Leo P or IZw18) would have a hotter temperature than its morphological counterpart in the LMC.

The 3000-3450 Å near-UV region for the $0.03Z_{\odot}$ models is shown in Fig. 6. As expected, the metallic lines are now significantly weaker, but there are still several weak O III lines present in the models corresponding to later O-types ($T_{\text{eff}} = 32,500$ & $35,000$). As with the He I/He II line ratios in the visible (Fig. 7), there is a shift in temperature of when the He I $\lambda 3188$ and He II $\lambda 3203$ lines have equivalent intensities at lower metallicity. They are roughly equivalent at $T_{\text{eff}} = 32,500$ in the $0.03Z_{\odot}$ models (Fig. 6), compared to somewhere between $T_{\text{eff}} = 32,500$ and $30,000$ in the $0.5Z_{\odot}$ models (Fig. 2). Again this reflects the hotter models needed to reproduce a given line ratio at lower metallicity (i.e. the temperature for a given spectral type, on the basis of using Galactic morphological criteria, would be higher).

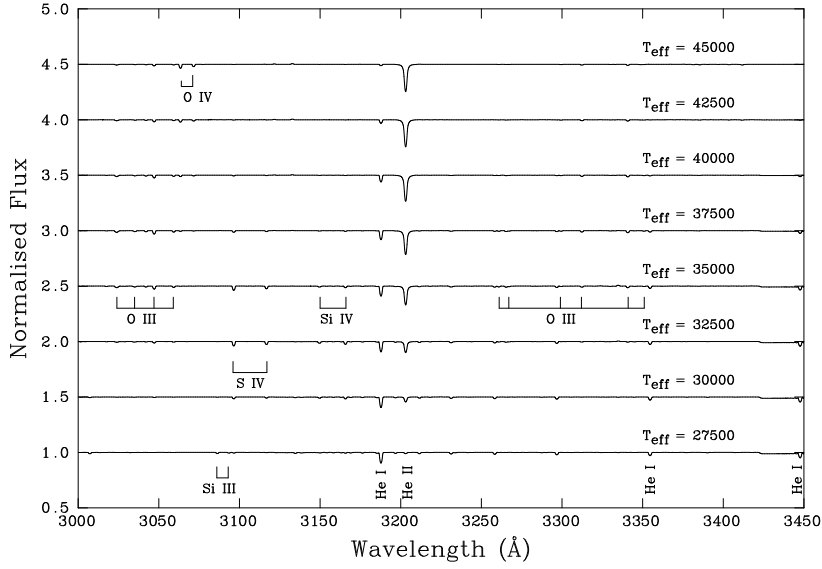


Fig. 6 Synthetic near-UV spectra from the TLUSTY $Z = 0.03Z_{\odot}$ OSTAR2002 grid, which have been convolved with a rotational-broadening function of $v \sin i = 100 \text{ km s}^{-1}$. Identified lines are: He I $\lambda\lambda 3188, 3355, 3448$; He II $\lambda 3203$; O III $\lambda\lambda 3024, 3035, 3047, 3059, 3261, 3267, 3299, 3312, 3341, 3351$; O IV $\lambda\lambda 3063, 3072$; Si III $\lambda\lambda 3086, 3093$; Si IV $\lambda\lambda 3150, 3166$; S IV $\lambda\lambda 3097, 3118$.

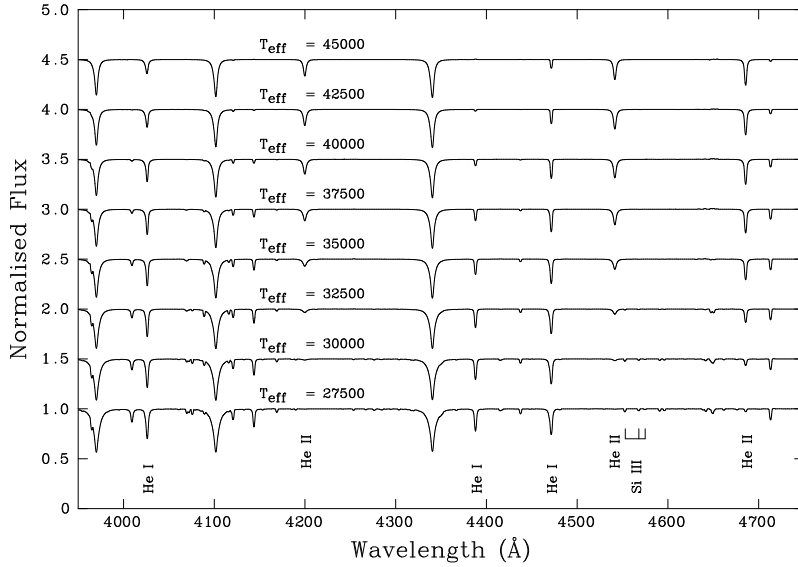


Fig. 7 Synthetic spectra from the TLUSTY $Z = 0.03Z_{\odot}$ OSTAR2002 grid for the traditional classification domain. The spectra have been convolved with a rotational-broadening function of $v \sin i = 100 \text{ km s}^{-1}$. Identified lines are the same as in Fig. 3.

4 Stellar properties in Local Group galaxies

4.1 Oxygen abundances

The key properties of a (single) massive star are defined by its initial mass and metallicity, but its path in the Hertzsprung–Russell diagram and ultimate fate depend critically on both mass loss and rotation [22,23]. Studies have shown that the effects of rotation are enhanced at low metallicity (e.g. [24, 25]), and rotationally-enhanced mixing is predicted to bring CNO-processed material to the stellar surface. To test the various implementations and prediction of rotation and mixing in stellar evolution models we require good empirical constraints of CNO abundances as a function of temperature, luminosity, metallicity and rotation rates.

As illustrated in Fig. 2, the near UV spectra of O-type stars contain a plethora of oxygen lines, with several O IV lines in the hottest spectra, a large number of O III lines in mid-late types, and weak O II lines in the coolest spectra (e.g. $\lambda 3390$). These lines are the best available diagnostics of O abundances in massive stars, because those at other wavelengths are generally saturated and strongly affected by stellar winds, making abundance determination both complicated and uncertain. Moreover, the use of multiple lines is also critical to arrive at accurate abundances with reliable error bars (see Fig. 1 from [26]). We add that accurate oxygen abundances are required to use the O V $\lambda 1371$ line from far-UV observations to estimate stellar wind densities around the sonic point and to explore the effect of clumping in the wind to arrive at reliable mass-loss rates. There are also useful lines from C and N in the near-UV range (e.g. C III $\lambda 3609$ and N III $\lambda\lambda 3354\text{--}67\text{--}74$) that appear to free of wind effects in relevant CMFGEN models (e.g. [27]), but these warrant further investigation.

To illustrate the sensitivity of the O III lines to abundance changes and the S/N of the observations, in Fig. 8 we show a CMFGEN model [10] with $T_{\text{eff}} = 31,000$ K and $\log(g) = 3.1$ for HD 269702 (classified as O8 I(f)p, see [28]) in the LMC. The baseline oxygen abundance is $12 + \log(\text{O}/\text{H}) = 8.39$ (shown in green), compared with models for $12 + \log(\text{O}/\text{H}) = 8.74$ (in red) and 7.78 (comparable to results for metal-poor irregulars, in black). We then introduced model noise to each spectrum to reproduce continuum S/N levels of 50, 100 and 150 as shown in the figure.

As expected given past observational studies (e.g. [26]), the spectra in Fig 8 suggest that $S/N \gtrsim 100$ is required to estimate O abundances in the LMC and more metal rich targets as the lines becomes saturated. For instance, there is little sensitivity to changes in abundance over this abundance range in the O III $\lambda 3312$ line. However, the situation is less challenging at lower abundances – although S/N remains critical, the lines are more responsive to abundance changes. As noted above, the precision on the estimated O abundance can also be improved by analysing multiple lines together (recalling the large number of O III lines in the mid-late O-type spectra in Fig. 2, and the O IV lines in the hottest spectra).

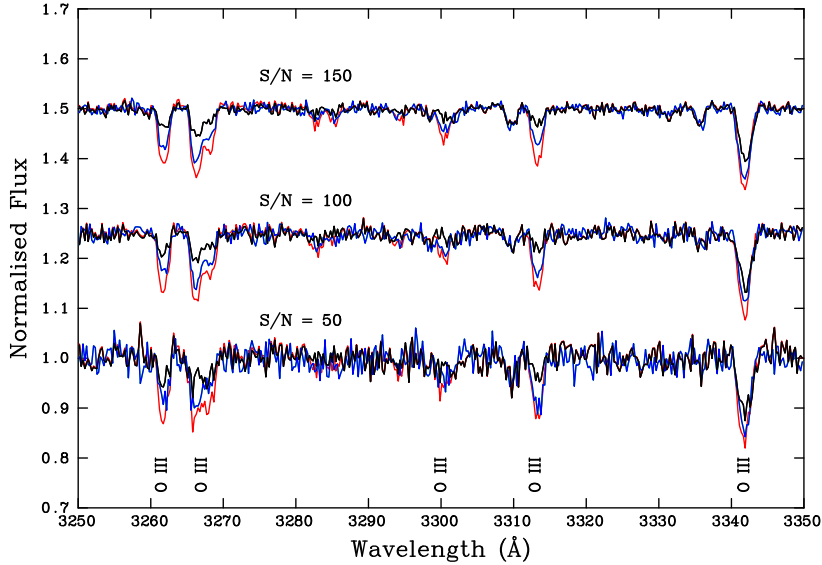


Fig. 8 The impact of noise on the O III lines in CMFGEN model spectra of an O8-type star in the LMC. Three oxygen abundances are shown, a LMC model with $12 + \log(\text{O}/\text{H}) = 8.39$ (blue), and models with $12 + \log(\text{O}/\text{H}) = 8.74$ (red) and 7.78 (black, comparable to results in WLM and NGC 3109) to illustrate the sensitivity of the lines. Identified lines are O III $\lambda\lambda 3261, 3267$ (blend), 3299, 3312, 3341. Noise has been added to the models to simulate different signal-to-noise (S/N) ratios in the continuum as indicated.

To date, estimates of O abundances in B-type supergiants have been possible in metal-poor galaxies at the fringes of the Local Group, e.g. $12 + \log(\text{O}/\text{H}) = 7.83 \pm 0.12$ in WLM [29] and 7.76 ± 0.07 in NGC 3109 [30]. Similar techniques were also used to estimate light-element abundances (C, N, O, Si, Mg) of B-type supergiants at ~ 2 Mpc in NGC 55 [31]. However, while the supergiants are a useful reference point for the evolutionary models (and for comparisons with nebular abundances), for true insights into the physical processes on the main sequence, we need similar studies of O-type stars. Even though we have confirmed O stars in WLM and NGC 3109 [29,30], as well as in IC 1613 [32] and Sextans A [33], abundance estimates are out of reach of present observations (e.g. [34,35]).

4.2 Stellar rotational velocities

Another important observational property of massive stars is their projected rotational velocity ($v \sin i$). As noted above, stellar rotation is important in the context of chemical enrichment (e.g. CNO abundances), and observational estimates of $v \sin i$ are also powerful diagnostics of rapidly-rotating stars that

have experienced chemically-homogeneous evolution or that have previously undergone binary interaction.

The helium lines in visible spectra are often used to estimate rotational velocities of O-type stars (e.g. [36]). Although they are affected by Stark broadening (typically with an equivalent FWHM of 50-100 km s⁻¹), the helium lines can be used to study the overall distribution of projected rotational velocities for samples of stars, while also allowing identification of rapid rotators. However, working with low-resolution ($R \sim 1000$) spectroscopy from, e.g. FORS2 or OSIRIS (on the Gran Telescopio Canarias), at S/N ~ 50 we are unable to put even modest constraints on $v \sin i$; the minimum combination required is $R > 2000$ and S/N > 100 .

A more robust probe of rotational velocities is provided by metallic lines in the spectra of massive stars. The metallic lines do not suffer from Stark broadening, nor do they suffer nebular contamination which can also hamper the use of helium lines in extragalactic targets. The visible spectra of B-type stars are replete with isolated metal lines that can be used to investigate $v \sin i$ (e.g. Si III, Si IV, Mg II etc) but the only comparably useful probe for O-type stars is the (less commonly observed) O III $\lambda 5591$ line.

The capabilities of CUBES are particularly compelling in this context. The combination of its sensitivity, improved spectral resolution (compared to e.g. FORS2) and access to the broad range of metallic lines in the near UV (see Fig. 3) will enable robust estimates of $v \sin i$ for metal-poor stars at the edge of the Local Group. High S/N observations would also enable investigation of the contribution of macroturbulent broadening in (sub-SMC) metal-poor O-type stars for the first time (e.g. [37, 38]). For instance, for stars with relative narrow lines, S/N $\gtrsim 100$ is sufficient to use Fourier transform analysis to estimate the contribution of macroturbulence [39].

4.3 Alternative temperature diagnostics

Beyond the O-type stars discussed here, the coverage of the Balmer jump provided by CUBES could also provide valuable constraints on effective temperature for other extragalactic targets, as used for e.g. A-type supergiants [47], B-type supergiants [48], and Be-type stars [49]. This technique typically requires accurate determination of the flux levels at either side of the Balmer limit, rather than precise absolute flux calibration. We do not explore this application further here, but note it for completeness and as an example of where flux calibration of the spectra will be important to have a good understanding of the wavelength-dependent properties of the spectra (response function, slit-losses etc).

5 CUBES Performances

In contrast to lower-mass stars, the spectral energy distributions of massive stars peak in the far-UV. This means that observations with CUBES will probe

the rising part of the flux distribution, potentially opening-up observations of targets that are otherwise too faint to observe with other facilities. For instance, the intrinsic $U-V$ colour for a mid O-type star is $(U-V)_0 \sim -1.5$ mag (e.g. [40]), representing a potentially significant gain compared to observations at visible wavelengths.

One caveat to this potential gain is the challenge of line-of-sight extinction towards potential targets, as its effects become more significant at shorter wavelengths (with $A(U) \approx 1.5 A(V)$ [41]). Nonetheless, most potential extragalactic targets are sufficiently far from the Galactic plane, such that foreground extinction will not be too much of a limiting factor, although targets in external galaxies might have to be carefully selected to avoid those with a significant local contribution to the line-of-sight extinction.

To estimate the potential performance of CUBES in the studies of O-type stars in galaxies such as IC 1613, WLM and NGC 3109 we used some of the model spectra discussed above as inputs to the Exposure Time Calculator (ETC) developed during the conceptual design phase [42]. The confirmed O-type stars in these irregular galaxies have $V = 19$ to 20.5 mag. The S/N predictions from the ETC for 2 hr exposures of three of the TLUSTY $0.5Z_{\odot}$ dwarf models are summarised in Table 1; adopted parameters for each calculation were: airmass = 1.2 (a reasonable assumption for the example galaxies), seeing = $0.8''$, spatial binning $\times 2$, spectral binning $\times 4$.

Given the similarity in the spectral energy distributions, the same ETC calculations using the $0.03Z_{\odot}$ are nearly identical in the predicted S/N, so the use of the LMC-like models here does not unduly influence the results. The S/N values are quoted for two wavelengths: 3195 \AA as representative of the continuum S/N near the He I $\lambda 3188$ and He II $\lambda 3203$ lines, and at 3640 \AA to indicate the S/N shortwards of the Balmer limit.

The image slicer for the low-resolution mode generates a wider effective slit such that the resulting spectra are oversampled (with >9 pixels per resolution element), hence the adopted $\times 4$ spectral binning in the calculations to bolster the resulting S/N without loss of resolution. Equally, for the faintest massive stars, we could bin by a further factor of two to improve the S/N (i.e. $\sqrt{2} \times S/N_{\text{ETC}}$), degrading the spectrum to an effective resolving power of $R \sim 3,500$ (still more than three times that obtained for 3 hr integrations of massive stars beyond 1 Mpc with FORS2, e.g. [30]). In the low-resolution mode the slicer has six $1''$ slices, so in the ETC calculations we only extracted the central two slices (to optimise the S/N).

With additional binning spectrally, the results in Table 1 demonstrate that it should be possible to obtain sufficient S/N ($\gtrsim 100$) for studies of the physical parameters and oxygen abundances of O-type stars in galaxies at the edges of the Local Group (i.e. 1.2-1.3 Mpc), with slightly longer (~ 2.5 -3 hr) exposures of the fainter known O stars in these systems.

Table 1 Signal-to-noise (S/N) predictions for CUBES observations of massive stars with the low-resolution mode for illustrative LMC-like ($Z = 0.5Z_{\odot}$) TLUSTY models. Adopted parameters for the Exposure Time Calculator (ETC) are: exposure time = 2 hr, airmass = 1.2, seeing = $0.8''$, spatial binning $\times 2$, spectral binning $\times 4$ (given that the low-resolution mode is sampled with >9 pixels per resolution element).

V (mag.)	$T_{\text{eff}} = 45.0 \text{ kK}$		$T_{\text{eff}} = 37.5 \text{ kK}$		$T_{\text{eff}} = 27.5 \text{ kK}$	
	S/N $_{\lambda 3195}$	S/N $_{\lambda 3640}$	S/N $_{\lambda 3195}$	S/N $_{\lambda 3640}$	S/N $_{\lambda 3195}$	S/N $_{\lambda 3640}$
19.0	95	113	93	111	86	104
19.5	74	88	72	86	66	81
20.0	57	67	55	66	50	62
20.5	43	51	42	50	38	47

5.1 ‘ELT science’ with the VLT

As an exciting example of where CUBES can bring observations into reach that are beyond our current capabilities, we highlight the case of star LP 26 in the dwarf Leo P galaxy [43]. Deep (8 hr) observations with the Multi-Unit Spectroscopic Explorer (MUSE) instrument revealed weak He II $\lambda\lambda 4686, 5411$ absorption lines, providing the first direct evidence of an O-type star in Leo P. This is particularly interesting as the significantly low oxygen abundance (3% solar) of the H II region in Leo P suggests it has a near-primordial composition [45].

Although relatively nearby (1.6 Mpc [44]) for such a metal-poor system, Leo P is sufficiently far away that further visible spectroscopy of its hot stars is beyond our current capability. For instance, the *HST* magnitudes for LP 26 are $F475W = 21.5$ and $F814W = 21.8$ (which, taking these as proxies for V and I filters compared to the anticipated intrinsic colours for O-type stars, suggest a low line-of-sight extinction). This puts it beyond the reach of (feasible) observing proposals with existing visible spectrographs, and further visible spectroscopy of the stellar population of Leo P was thought to have to wait until the Extremely Large Telescope (ELT) is operational.

First constraints on the properties of LP 26 have recently been provided by analysis of far-UV *HST* spectroscopy, reporting a fast rotational velocity ($v \sin i = 370 \pm 90 \text{ km s}^{-1}$) and, as expected given the lower metallicity, weaker wind lines than in comparison templates of SMC stars [46]. Using the same OSTAR2002 TLUSTY grid as in our calculations, the far-UV spectroscopy was combined with multiband photometry to estimate its temperature as $T_{\text{eff}} = 37,500 \text{ K}$, with uncertainties of order $\pm 6 \text{ kK}$.

The near-UV lines identified in the CUBES range offer the prospect of characterising the physical properties of LP 26. We used the 3% solar $T_{\text{eff}} = 37,500 \text{ K}$ TLUSTY model to estimate the performance for $V = 21.5 \text{ mag.}$ with the ETC. The same parameters were used as in Table 1, including airmass = 1.4, as this corresponds to the maximum altitude that Leo P (with a declination of $+18^\circ$) reaches from Paranal. Extracting only the central two slices again, the ETC predicts $S/N = 34$ at 3640 \AA in a total integration of 4 hrs; binning this (spec-

trally) by a further factor of two would provide $S/N \sim 50$ in a relatively modest half night of observations; the same calculation for 3195 \AA (central slice only, binning the ETC results by a further factor of two yields $S/N \sim 40$).

Such an observation would enable estimates of the physical parameters (temperature, gravity) of LP 26 in a relatively modest amount of observing time (half a night). This nicely illustrates the potential of CUBES in this scientific area – we expect more candidate O-type stars to be discovered in the coming years at 1 Mpc and beyond, and CUBES could provide a powerful capability to constrain their physical parameters.

Direct determination of the oxygen abundance at the low metallicity of Leo P will, however, remain challenging. The metal lines are sufficiently weak that greater S/N (> 100) is required for secure detections. To explore this further, in Fig. 9 we show the same TLUSTY model spectrum for the O III lines in the $3250\text{-}3350 \text{ \AA}$ region. A continuum S/N in excess of 100 is required to tentatively detect the O III $\lambda 3341$ line, with $S/N = 150$ being a more realistic goal if equivalent widths (or even firm upper limits) were to be measured. From the ETC, recovering a S/N of order 150 at 3350 \AA (assuming the same binning as above in the ETC, and a further factor of $\sqrt{2}$) would require a total integration of ~ 45 hr. Such an ambitious observation is unlikely to be feasible, particularly given e.g. systematics that might limit performance from combining a large number of exposures together, although we will re-assess this case later in the construction phase of CUBES.

5.2 Impact of O_3 absorption

Shortwards of $\sim 3400 \text{ \AA}$ the extinction due to atmospheric ozone (O_3) becomes a significant factor, with a steep dependence of the extinction as a function of airmass (see e.g. Fig. 2 from [50]). Within this region there are also discrete O_3 bands, which can impact on the study of potential stellar features. In the context of the potential diagnostic lines discussed here, it is notable that one of the bands spans the (rest-frame) He II $\lambda 3203$ line (e.g. Fig. 1 from [5]). Although weaker at the longer wavelengths, careful correction for the O_3 bands will also be required to study the O III features discussed above,

On this topic we note the study by [51] who used historic stellar spectroscopy to recover information on the intensity of past O_3 features; this highlighted that with careful modelling (helped in this particular case by near-UV HST observations) the stellar features could be removed successfully to reveal the O_3 band absorption; the reverse would also be true in terms of recovering the intrinsic stellar spectra.

The operational concept for CUBES is under development as the project progresses, but careful subtraction of the O_3 features will be an important consideration. The current plans include observations of flux standards (with high signal-to-noise) to help reconstruct the atmospheric absorption features, combined with using theoretical tools such as MOLECFIT [52].

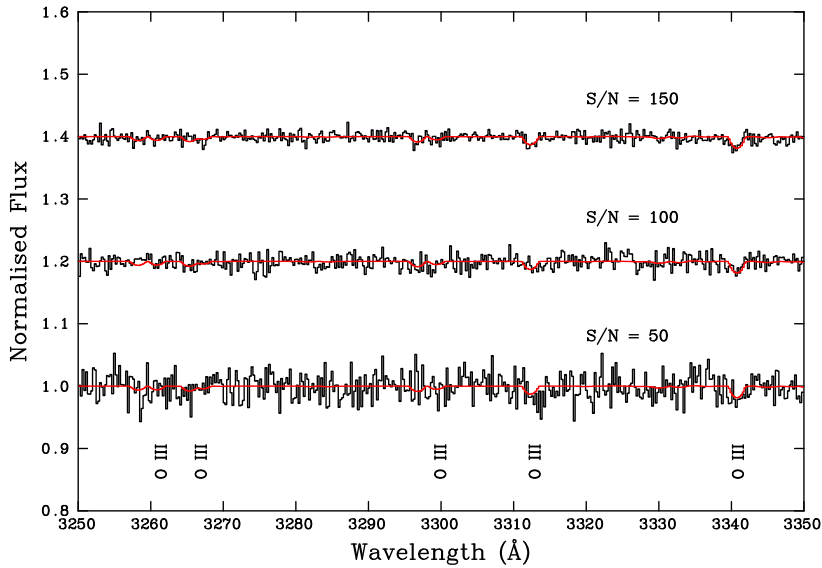


Fig. 9 Synthetic TLUSTY spectra ($Z = 0.03Z_{\odot}$, $T_{\text{eff}} = 37,500$, $\log g = 4.0$) to investigate the potential of recovering oxygen abundances for different levels of simulated signal-to-noise (S/N) in the test case for Leo P (see Section 5). The spectra with added noise are shown in black, with the original model spectrum overplotted on each in red. The identified O III lines are the same as those in Fig. 8.

6 Summary

We have used model atmospheres to investigate the spectral diagnostics available over the 3000-4050 Å range that will be accessible with the new CUBES instrument now in development for the VLT. There have been relatively few studies of OB-type stars shortwards of the Balmer limit at (ground) near UV wavelengths to date, but CUBES will provide an exciting new capability to study massive stars in metal-poor systems at the edge of the Local Group and beyond.

Following the pioneering work from [5], the He I $\lambda 3188$ and He II $\lambda 3203$ pair of lines appear to be a compelling diagnostic of stellar temperature, with the high Balmer series of lines providing constraints on gravity. The near UV is also rich with metallic lines (O III, O IV, Si III, Si IV, N III) that can provide further temperature diagnostics (where more than one ionisation stage is present for a given element) as well as estimates of chemical abundances in O-type stars, particularly for oxygen where we lack robust diagnostics at visible wavelengths.

Our results from the ETC presented here demonstrate that it should be possible with CUBES to obtain high-quality ($S/N > 100$, $R \sim 7,000$) near-UV spectra of massive O-type stars in metal-poor systems at ~ 1 Mpc in ~ 3 hr integrations. The CUBES analysis will probably be informed by initial estimates

of stellar parameters from observations at other wavelengths, and will provide further constraints on stellar temperatures and gravities, together with estimates of projected rotational velocities and the first oxygen abundances for O-type stars in these extragalactic systems. Such results will enable much needed comparisons with theoretical predictions from low-metallicity evolutionary models and perhaps the first observational evidence for chemically-homogeneous evolution. Furthermore, using very metal-poor model spectra (with $Z = 0.03Z_{\odot}$) we have shown that CUBES could obtain spectra with $S/N \sim 50$ of the candidate O-type star in Leo P at 1.6 Mpc in approximately half a night of observations.

Our qualitative consideration of the models here was intended as a first study of the potential diagnostics available in the CUBES domain. Data from the ongoing XShootU ESO Large Programme (in support of the *HST* ULLYSES Legacy Survey) will soon enable quantitative investigation of O-type spectra in the CUBES region from high S/N (> 100) X-Shooter observations in the Magellanic Clouds. Analysis of the XShootU data will provide an important test of the temperatures estimated using the He I $\lambda 3188$ /He II $\lambda 3203$ ratio and $\log g$ from the high Balmer lines compared to diagnostics in the visible. Our expectation is that for the extragalactic metal-poor dwarfs envisaged as future CUBES targets, the impact of stellar winds on the determination of physical parameters from the near-UV region alone should be relatively minor, and the XShootU data in the Clouds will provide an important test of this.

More generally, the greater throughput and resolving power delivered by CUBES compared to X-Shooter will give a unique capability for studies of massive stars in the ground-UV region. Moreover, the absence of cross-dispersion in the CUBES design will avoid the challenges of blaze correction and order recombination that affect the analysis of data from echelle instruments such as UVES and X-Shooter; the CUBES design will give a smooth, continuous spectral response for the two optical channels. This will enable more robust definition of the stellar continuum for normalization, particularly for broad features in the Balmer line series, as well as analysis of weaker absorption lines if they would otherwise be in the reconnection regions. The latter will be important for more rapidly-rotating massive stars ($v \sin i \gtrsim 100 \text{ km s}^{-1}$), which will also benefit from the greater resolving power compared to X-Shooter.

Acknowledgements We thank the reviewers for their suggestions on the manuscript, which helped clarify details as well as helping place this study in the wider context of previous work and some of the challenges of ground-based observations at these short wavelengths. MG acknowledges financial support from grants ESP2017-86582-C4-1-R and PID2019-105552RB-C41, and from the Unidad de Excelencia “María de Maeztu” – Centro de Astrobiología (CSIC-INTA) project, MDM-2017-0737.

Conflict of interest

The authors declare that they have no conflict of interest.

Data availability statement

The TLUSTY models used in this article are freely available online. The UVES data of HDE 269896 and the CMFGEN models shown in Figs. 1 and 8 are available on request.

References

1. Walborn, N. R. & Fitzpatrick, E. L.: Contemporary Optical Spectral Classification of the OB Stars: A Digital Atlas. *PASP*, 102, 379 (1990)
2. Puls, J., Kudritzki, R.-P., Herrero, A. et al.: O-star mass-loss and wind momentum rates in the Galaxy and the Magellanic Clouds Observations and theoretical predictions. *A&A*, 305, 171 (1996)
3. Zanutta, A., Cristiani, S., Atkinson, D. et al.: CUBES Phase A design overview. *ExA*, 55, 241 (2023)
4. Lamers, H. J.: The spectrum of the supergiant ϵ Orionis (B0 Ia). I. Identifications, equivalent-widths, line profiles. *A&AS*, 7, 113 (1972)
5. Morrison, N. D.: The lines He I λ 3187 and He II λ 3203 in O-type stars *ApJ*, 202, 433 (1975)
6. Dufton, P. L. & McKeith, C. D.: Copernicus observations of neutral helium lines in early-type stars. *A&A*, 81, 8 (1980)
7. Drissen, L., Moffat, A. F. J., Walborn, N. R. & Shara, M. M.: The Dense Galactic Starburst NGC 3603. I. HST/FOS Spectroscopy of Individual Stars in the Core and the source of Ionization and Kinetic Energy. *AJ*, 110, 2235 (1995)
8. Walborn, N. R. & Howarth, I. D.: Digital Spectroscopy of O3-O5 and ON/OC Supergiants in Cygnus. *PASP*, 112, 1446 (2000)
9. Evans, C. J., Crowther, P. A., Fullerton, A. W. & Hillier, D. J.: Quantitative Studies of the Far-Ultraviolet, Ultraviolet, and Optical Spectra of Late O- and Early B-Type Supergiants in the Magellanic Clouds. *ApJ*, 610, 1021 (2004)
10. Hillier, D. J. & Miller, D. L.: The Treatment of Non-LTE Line Blanketing in Spherically Expanding Outflows. *ApJ*, 496, 407 (1998)
11. Lanz, T. & Hubeny, I.: A Grid of Non-LTE Line-blanketed Model Atmospheres of O-Type Stars. *ApJS*, 146, 417 (2003)
12. Evans, C. J., Lennon, D. J., Langer, N. et al.: The VLT-FLAMES Tarantula Survey. *Msngr*, 181, 22 (2020)
13. Grevesse, N. & Sauval, A.: Standard solar composition *SSRv*, 85, 161, (1998)
14. Sabín-Sanjulián, C., Simón-Díaz, S., Herrero, A. et al.: The VLT-FLAMES Tarantula Survey. XXVI. Properties of the O-dwarf population in 30 Doradus. *A&A*, 601, A79 (2017)
15. Trundle, C., Dufton, P. L., Hunter, I. et al.: The VLT-FLAMES survey of massive stars: evolution of surface N abundances and effective temperature scales in the Galaxy and Magellanic Clouds. *A&A*, 471, 625 (2007)
16. Sota, A., Maíz Apellániz, J., Walborn, N. R. et al.: The Galactic O-Star Spectroscopic Survey. I. Classification System and Bright Northern Stars in the Blue-violet at $R \sim 2500$. *ApJS*, 193, 24 (2011)
17. Markova, N., Puls, J., Scuderi, S. et al.: Spectroscopic and physical parameters of Galactic O-type stars. I. Effects of rotation and spectral resolving power in the spectral classification of dwarfs and giants. *A&A*, 530, A11 (2011)
18. Arias, J. I., Walborn, N. R., Simón-Díaz, S. et al.: Spectral classification and properties of the O Vz stars in the Galactic O-Star Spectroscopic Survey (GOSSS) *AJ*, 152, 31 (2016)
19. Ramírez-Agudelo, O. H., Sana, H., de Koter, A. et al.: The VLT-FLAMES Tarantula Survey . XXIV. Stellar properties of the O-type giants and supergiants in 30 Doradus. *A&A*, 600, A81 (2017)
20. Garcia, M., Evans, C. J., Bestenlehner, J. M. et al.: Massive stars in extremely metal-poor galaxies: a window into the past. *ExA*, 51, 887 (2021)
21. Szécsi, D., Langer, N., Yoon, S.-C. et al.: Low-metallicity massive single stars with rotation. Evolutionary models applicable to I Zwicky 18. *A&A*, 581, A15 (2015)

22. Puls, J., Vink, J. S. & Najarro, F.: Mass loss from hot massive stars. *A&ARv*, 16 209 (2008)
23. Langer, N.: Presupernova Evolution of Massive Single and Binary Stars *ARA&A*, 50, 107, (2012)
24. Maeder, A. & Meynet, G.: Stellar evolution with rotation. VII. Low metallicity models and the blue to red supergiant ratio in the SMC. *A&A*, 373, 555 (2001)
25. Brott, I., de Mink, S. E., Cantiello, M. et al.: Rotating massive main-sequence stars. I. Grids of evolutionary models and isochrones. *A&A*, 530, A115 (2011)
26. Martins, F., Hervé, A., Bouret, J.-C. et al.: The MiMeS survey of magnetism in massive stars: CNO surface abundances of Galactic O stars. *A&A*, 575, A34 (2015)
27. Marcolino, W. L. F., Bouret, J.-C., Rocha-Pinto, H. J. et al.: Wind properties of Milky Way and SMC massive stars: empirical Z dependence from CMFGEN models *MNRAS*, 511, 5104 (2022)
28. Walborn, N. R., Howarth, I. D., Evans, C. J. et al.: The Onfp Class in the Magellanic Clouds. *AJ*, 139, 1283 (2010)
29. Bresolin, F., Pietrzyński, G., Urbaneja, M. A. et al.: The Araucaria Project: VLT Spectra of Blue Supergiants in WLM- Classification and First Abundances. *ApJ*, 648, 1007 (2006)
30. Evans, C. J., Bresolin, F., Urbaneja, M. A. et al.: The ARAUCARIA Project: VLT-FORS Spectroscopy of Blue Supergiants in NGC 3109 – Classifications, First Abundances, and Kinematics. *ApJ*, 659, 1198 (2007)
31. Castro, N., Urbaneja, M. A., Herrero, A. et al.: The ARAUCARIA project: Grid-based quantitative spectroscopic study of massive blue stars in NGC 55. *A&A*, 542, A79 (2012)
32. García, M. & Herrero, A.: The young stellar population of IC 1613. III. New O-type stars unveiled by GTC-OSIRIS. *A&A*, 551, A74 (2013)
33. Camacho, I., García, M., Herrero, A., & Simón-Díaz, S.: OB stars at the lowest Local Group metallicity. GTC-OSIRIS observations of Sextans A. *A&A*, 585, A82 (2016)
34. Tramper, F., Sana, H., de Koter, A. & Kaper, L.: On the Mass-loss Rate of Massive Stars in the Low-metallicity Galaxies IC 1613, WLM, and NGC 3109. *ApJ*, 741, L8 (2011)
35. Tramper, F., Sana, H., de Koter, A. et al.: The properties of ten O-type stars in the low-metallicity galaxies IC 1613, WLM, and NGC 3109. *A&A*, 572, A36 (2014)
36. Ramírez-Agudelo, O. H., Simón-Díaz, S., Sana, H. et al.: The VLT-FLAMES Tarantula Survey. XII. Rotational velocities of the single O-type stars. *A&A*, 560, A29 (2013)
37. Aerts, C., Puls, J., Godart, M. & Dupret, M. A.: Collective pulsational velocity broadening due to gravity modes as a physical explanation for macroturbulence in hot massive stars. *A&A*, 508, 409 (2009)
38. Simón-Díaz, S., Herrero, A., Uytterhoeven, K. et al.: Observational Evidence for a Correlation Between Macroturbulent Broadening and Line-profile Variations in OB Supergiants. *ApJ*, 720, L174 (2010)
39. Simón-Díaz, S. & Herrero, A.: The IACOB project. I. Rotational velocities in northern Galactic O- and early B-type stars revisited. The impact of other sources of line-broadening. *A&A*, 562, A135 (2014)
40. Johnson, H. L.: Astronomical Measurements in the Infrared. *ARA&A*, 4, 193 (1966)
41. Cardelli, J. A., Clayton, G. C. & Mathis, J. S.: The Relationship between Infrared, Optical, and Ultraviolet Extinction. *ApJ*, 345, 245 (1989)
42. Genoni, M., Landoni, M., Cupani, G. et al.: The CUBES Instrument Model and Simulation Tools. *ExA*, 55, 301 (2023)
43. Evans, C. J., Castro, N., Gonzalez, O. A. et al.: First stellar spectroscopy in Leo P. *A&A*, 622, A129 (2019)
44. McQuinn, K. B. W., Skillman, E. D., Dolphin, A. et al.: Leo P: An Unquenched Very Low-mass Galaxy. *ApJ*, 812, 158 (2015)
45. Skillman, E. D., Salzer, J. J., Berg, D. A. et al.: ALFALFA Discovery of the nearby Gas-rich Dwarf Galaxy Leo P. III. An Extremely Metal Deficient Galaxy. *AJ*, 146, 3 (2013)
46. Telford, G. O., Chisholm, J., McQuinn, K. B. W. & Berg D.: Far-ultraviolet Spectra of Main-sequence O Stars at Extremely Low Metallicity. *ApJ*, 922, 191 (2021)
47. Kudritzki, R.-P., Urbaneja, M., Bresolin, F. et al.: Quantitative Spectroscopy of 24 A Supergiants in the Sculptor Galaxy NGC 300: Flux-weighted Gravity-Luminosity Relationship, Metallicity, and Metallicity Gradient. *ApJ*, 681, 269 (2008)

-
48. Zorec, J., Cidale, L., Arias, M. L. et al.: Fundamental parameters of B supergiants from the BCD system. I. Calibration of the (λ_1 , D) parameters into T_{eff} . *A&A*, 501, 297 (2009)
 49. Shokry, A. Rivinius, Th, Mehner, A. et al.: Stellar parameters of Be stars observed with X-shooter. *A&A*, 609, A108 (2018)
 50. Patat, F., Moehler, S., O'Brien, K. et al.: Optical atmospheric extinction over Cerro Paranal. *A&A*, 527, A91 (2011)
 51. Griffin, R. E.: The detection and measurement of telluric ozone from stellar spectra. *PASP*, 117, 885 (2005)
 52. Smette, A., Sana, H., Noll, S. et al.: Molecfit: A general tool for telluric absorption correction. I. Method and application to ESO instruments. *A&A*, 576, A77 (2015)